Oxime-Induced Reactivation of Sarin-Inhibited AChE: A Theoretical Mechanisms Study

ARTICLE *in* THE JOURNAL OF PHYSICAL CHEMISTRY B · APRIL 2007

Impact Factor: 3.3 · DOI: 10.1021/jp067741s · Source: PubMed

Oxime-Induced Reactivation of Sarin-Inhibited AChE: A Theoretical Mechanisms Study

Jing Wang,[†] Jiande Gu,*[,†,‡] Jerzy Leszczynski,*[,†] Mikolaj Feliks,[§] and W. Andrzej Sokalski[§]

Computational Center for Molecular Structure and Interactions, Department of Chemistry, Jackson State University, Jackson, Mississippi 39217, Drug Design and Discovery Center, State Key Laboratory of Drug Research, Shanghai Institute of Materia Medica, Shanghai Institutes for Biological Sciences, Chinese Academy of Sciences, Shanghai 201203, People's Republic of China, and Molecular Modeling and Quantum Chemistry Group, Institute of Physical and Theoretical Chemistry, Wrocław University of Technology, Wyb. Wyspianskiego 27, 50-370 Wrocław, Poland

Received: November 21, 2006; In Final Form: January 12, 2007

Oximes (especially oximate anions) are used as potential reactivators of OP-inhibited AChE due to their unique α-effect nucleophilic reactivity. In the present study, by applying the DFT approach at the B3LYP/6-311G(d,p) level and the Møller−Plesset perturbation theory at the MP2/6-311G(d,p) level, the formoximate-induced reactivation patterns of the sarin-AChE adduct and the corresponding reaction mechanism have been investigated. The potential energy surface along the pathway of the reactivation reaction of sarin-inhibited AChE by oxime reveals that the reaction can occur quickly due to the relatively low energy barriers. A two-step process is a major pathway proposed for the studied reactivation reaction. Through the nucleophilic attack, the oximate first binds to the sarin-AChE adduct to form a relatively stable phosphorus complex. The regeneration of the serine takes place subsequently through an elimination step, which is expected to be competitive with the nucleophilic attacking process. The polarizable continuum model (PCM) has been applied to evaluate the solvate effects on the pathway. It is concluded that the reaction energy barriers are also low enough for the reaction to easily occur in solvent. The results derived from both the gas-phase model and the aqueous solvation model suggest that the studied oximate anion is an efficient antidote reagent for sarin-inhibited AChE.

Introduction

Acetylcholinesterase (AChE)[1−5] is one of the serine hydralases. It catalyzes the hydrolysis of the neurotransmitter acetylcholine and terminates the impulse transmission at cholinergic synapses. As acute toxins, organophosphate esters (OPs) irreversibly inhibit AChE. OPs react directly with the hydroxyl of the serine in the catalytic triad of the active site of AChE to form relatively stable phosphorylated OP-AChE adducts, leading to fatal toxic effects on the active enzyme action.[6,7] Sarin (GB, i.e., *O*-isopropylmethylphosphonofluoridate), an extremely toxic nerve agent, is one of the well-characterized OP-type inhibitors. By inhibiting AChE, sarin disrupts the nervous system of a living organism, which causes the victim to be comatose and suffocate in a series of convulsive spasms.

The phosphorylated OP-AChE adduct either encounters the process of dealkylation aging or undergoes reactivation by various antidotes. In the former case, the phosphoester C−O bond other than the phosphoserine P−O bond is cleaved, and the irreversible loss of enzyme activity of AChE is observed. In the latter case, the enzyme is able to regain its enzymic activity. Reactivation of OP-inhibited AChE is therefore a primary goal in the treatment of OP poisoning. During the past several decades, effective therapeutic measures (antidotes) for OP poisoning have been actively sought both in vitro and in vivo. Because of its unique α-effect nucleophilic reactivity,[8,9] oximes (especially oximate anions) have long been used as potential reactivators of OP-inhibited AChE.[10,11] The studies of the OP-inhibited native, wild-type, and mutant recombinant DNA-expressed AChEs have established the relationship between the edrophonium acceleration of oxime-induced reactivation of the OP-AChE adducts and the phosphoryl oxime inhibition of the reactivated enzyme, which occurs during reactivation by the pyridinum oximes LüH6 and TMB4.[12]

Taylor and co-workers reported the reactivation of a series of resolved enantiomeric methylphosphonate adducts of AChE by two oximes, 2-pralidoxime (2-PAM) and 1-(2′-hydroxyiminomethyl-1′-pyridinium)-3-(4′carbamoyl-1-pyridinium) (HI-6).[13] Their studies suggested that the impact of the complexed organophosphate within the constraints of the active center gorge is a major factor in influencing oxime access and reactivation rates and that the efficiency of individual oximes as reactivating agents depends on the steric bulk of the intervening groups surrounding the tetrahedral phosphorus. On the other hand, the reactivation potency of four quaternary pyridine aldoximes for nerve agent intoxications were examined by using standard in vitro reactivation tests.[14] The results showed that none of these tested AChE reactivators was able to reactivate AChEs that are inhibited by all nerve agents. Different oximes exhibit various antidote effects on the OP-inhibited AChE.

An insight that provides the details of the mechanisms is essential for the understanding of the OP-inhibited AChE reactivation induced by the oxime class of species and for the development of more effective antidotes. Study of the mechanisms of the simplest member of the oxime family, formaldehyde oximate (formoximate), in the reactivation of the OP-AChE adducts provides the first key step toward better understanding

* Corresponding authors. E-mail: (J.G.) jiandegush@go.com and (J.L.) jerzy@ccmsi.us.
[†] Jackson State University.
[‡] Chinese Academy of Sciences.
[§] Wrocław University of Technology.

10.1021/jp067741s CCC: $37.00
Published on Web 02/14/2007

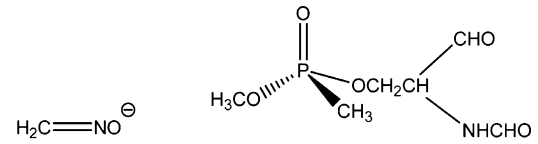

Figure 1. Reactant structures (oximate anion and sarin−serine adduct).

of the countermeasure role of the oxime family in restoring the catalytic activity of the OP-inhibited AChE. In the present study, the formoximate-induced reactivation patterns of the sarin-AChE adduct and the corresponding reaction mechanism have been investigated by the density functional theory (DFT) and the Møller−Plesset perturbation theory. The results derived from both the gas-phase model and the aqueous solvation model suggest that the oximate anion might be a promising antidote reagent for sarin-inhibited AChE.

Materials and Methods

Density functional theory (DFT) with Becke's three parameter (B3)[15] exchange functional along with the Lee−Yang−Parr (LYP)[16,17] nonlocal correlation functional (B3LYP) was employed in this study. The standard valence triple-ζ basis set, augmented with d-type polarization functions for heavy elements and p-type polarization functions for H, 6-311G(d,p),[18] was used. All of the studied models have been fully optimized by the analytic gradient techniques. In the analysis of harmonic vibrational frequency, the force constants were determined analytically for all of the complexes. The stationary structures were found by ascertaining that all of the harmonic frequencies were real. The structures of the transition states were obtained by verifying that one of the harmonic frequencies is imaginary and also by carrying out the intrinsic reaction coordinate (IRC) analysis for the reaction pathways. To verify the reliability of the DFT predictions, the second-order Møller−Plesset perturbation method with the same basis set (6-311G(d,p)) was also used to determine the structures and energies of the local minima and the corresponding transition states.[19] Natural population atomic (NPA) charges were determined using the same theoretical level with the natural bond orbital (NBO) analysis of Reed and Weinhold.[20−23] All DFT computations were performed by using the Gaussian 03 package of programs.[24] The polarizable continuum model (PCM) self-consistent reaction field of Tomasi and co-workers with a dielectric constant $\epsilon = 78.39$ (water)[25] was applied for all gas-phase optimized structures to evaluate the solvation effects on the potential energy surface of the reaction.

Results and Discussion

The reactivation of the OP-inhibited AChE considerably depends on the properties of the antidotes, such as the nucleophility and the orientation of the nucleophilic reagents. Various groups attached to the C atom of oximes are expected to change the reactivation ability of the reagents either through altering the nucleophility of the oxygen of the oximes or by changing their orientations. To explore the intrinsic properties of the reactivation mechanisms, the simplest oximate, formaldehyde oximate (formoximate) anion ($CH_2 = NO^-$), is a suitable model in the study of the role of the oxime family in the reactivation of the sarin-inhibited AChE addut. For the sarin-AChE adduct, the isopropyl group of the sarin moiety was modeled by a methyl group. The structures and labels of the reactants (oxime and sarin−serine adduct) are illustrated in Figure 1.

Being a nucleophilic reaction, the recreation process may undergo two possible pathways (depicted in Scheme 1). One of the pathways may proceed via a one-step reaction in which the nucleophilic attack of the oximate on the phosphonylated AChE and the departure of the serine moiety take place simultaneously (Scheme 1A).[9,10] The other pathway could go through a two-step reaction in which the oximate binds to the OP-AChE adduct to form a pentacoordinated phosphorus complex as a relatively stable intermediate and the regeneration of the serine occurs subsequently (Scheme 1B). Our previous study[6] on the mechanisms of the phosphonylated AChE induced by sarin suggested that the two-step mechanisms might be favored.

In the present investigation, four intermediates structures have been located as local minima on the potential energy surface (PES). Three corresponding transition states that link these intermediates have also been located as the first-order stationary points (shown in Figure 2).

When reactants (formoximate anion and sarin−serine adduct) mix together, they form a near attacking conformer (NAC)[26] (labeled as intermediate INT1 on the PES), which is 31 kcal/mol more stable than the separated reactants. It should be noted that the dipole moment of the sarin−serine adduct amounts to 6.3 D. Obviously, the charge−dipole interaction between oximate and sarin−serine adduct accounts for this large stabilization energy. Besides, two hydrogen bonds are shown in this INT1 complex. The oxygen (O1) of the formoximate and the hydrogen H1 of the methyl group of the sarin−serine adduct form a C−H···O-type of H-bond, with an O1···H1 distance of 1.796 Å. This H-bond is significantly stronger than the usual C−H···O-type hydrogen bonding. The natural bond orbital (NBO) analysis shows that its Wiberg bond index amounts to 0.11 au. This strong H-bond should be attributed to the negative charge residing on O1. Another C−H···N-type H-bond has been found for N1 of the oxime and H2 of the methoxyl group of the sarin moiety (the atomic distance is 2.163 Å). This H-bond is much weaker than the C−H1···O1. The atomic distance between O1 and phosphorus amounts to 3.892

SCHEME 1: Two Possible Reactivation Pathways of Sarin-Inhibited AChE Induced by Formoximate Anion

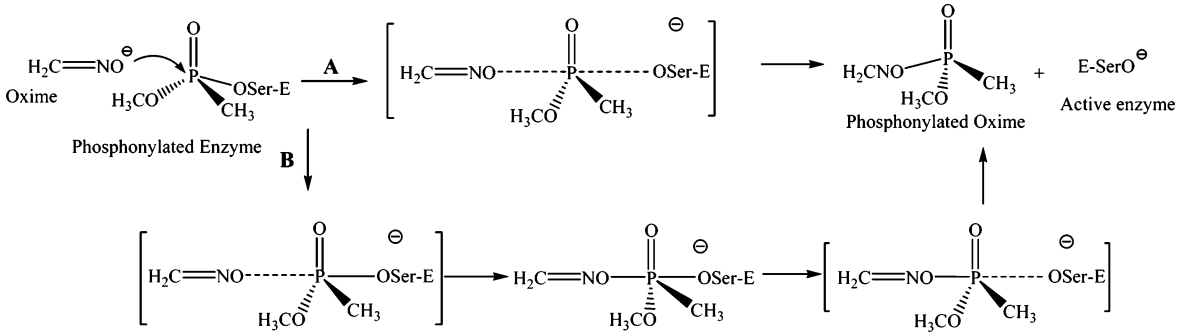

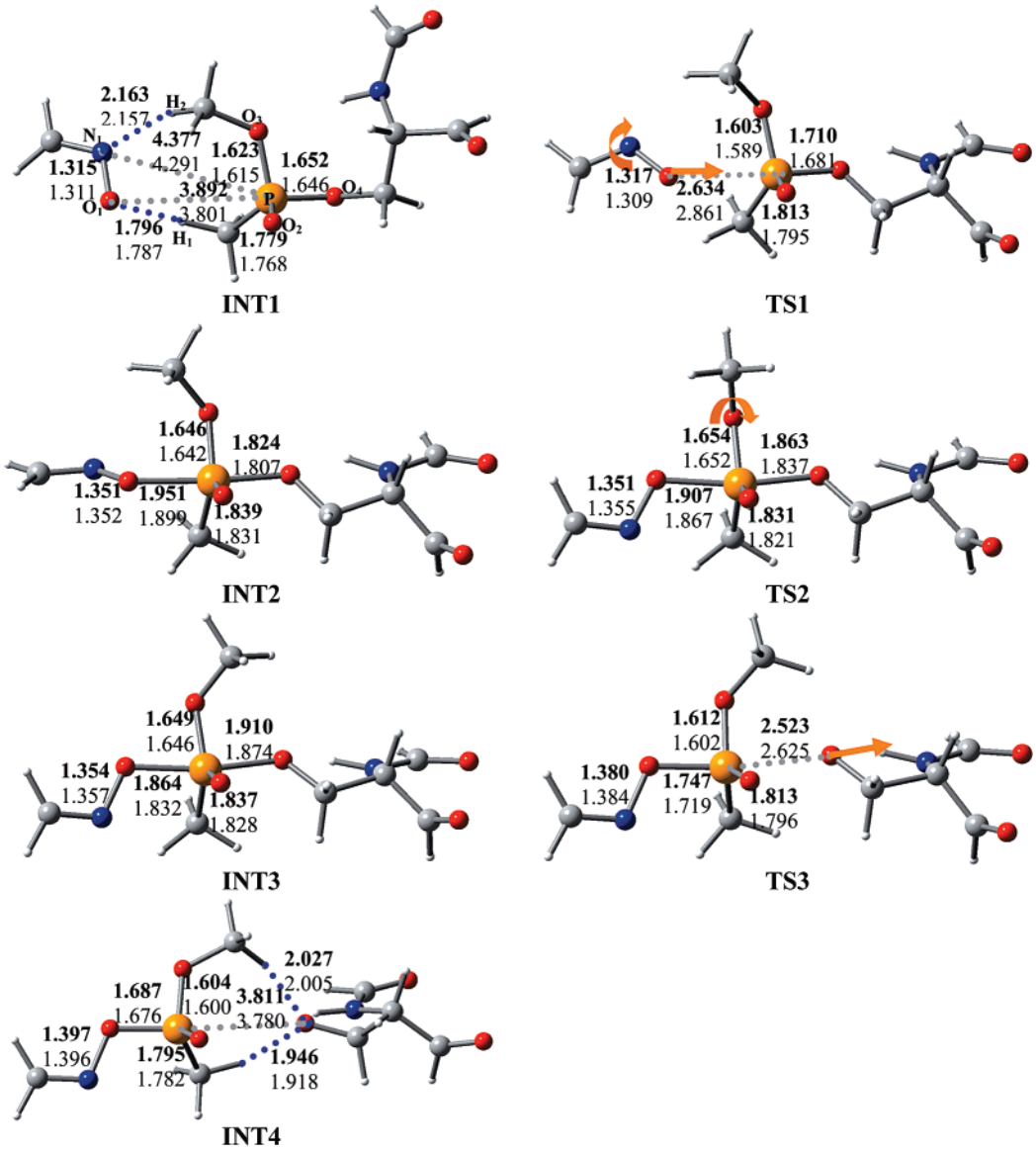

Figure 2. Optimized structures of intermediates and transiton states on the potential energy surface at the B3LYP/6-311G(d,p) and MP2/6-311G-(d,p) levels. Atomic distances in angstroms, DFT results in bold, and MP2 results in normal text. INT represents the intermediate, and TS represents the transiton state. Orange arrows reveal the imaginary vibrational mode of the transition states. H-bonds in blue dashes, C in gray, H in white, P in light orange, O in red, and N in blue.

TABLE 1: Energy Properties of Predicted Minima and Transition State Structures at B3LYP/6-311G(d,p) and MP2/6-311G(d,p) Levels (kcal/mol)

structures	ΔE	ΔE_{ZPE}	ΔG^0	ΔE_{PCM}
INT1[a]	0.0 (−1177.66474 au) *(−1174.92416* au)	0.0 (−1177.43974 au)	0.0 (−1177.49186 au)	0.0 (−1177.75676 au)
TS1	5.5 (*4.8*)	5.7	6.4	4.1
INT2	0.8 (*−3.2*)	1.3	2.8	1.1
TS2	0.9 (*−2.1*)	1.2	3.3	2.8
INT3	−0.1 (*−4.0*)	0.4	1.8	1.2
TS3	2.8 (*2.2*)	2.3	3.5	7.1
INT4	−2.6 (*−0.6*)	−3.3	−4.3	2.8

[a] The energy differences are calculated based on the energy value of INT1 (in parentheses). Italic values in parentheses represent results obtained from the MP2/6-311G(d,p) level.

Å. The bond length of the phosphor−serine P−O4 bond is calculated to be 1.652 Å in INT1, which is only 0.03 Å longer than that in the individual sarin−serine adduct (1.623 Å). The natural population atomic (NPA) charges on O1 and O4 are −0.67 and −0.84 au, respectively.

The transition state (TS1) for the nucleophilic attack step was found to be 5.5 kcal/mol (5.7 kcal/mol after the zero point correction, as listed in Table 1) above the INT1 on the potential energy surface of the reaction pathway. The single imaginary frequency of TS1 is calculated to be 84*i* cm^{-1}. The corresponding vibrational mode exhibits an assorted movement, demonstrating the direct linear nucleophilic attack of oxygen O1 of the formoximate toward the phosphorus atom of the sarin−serine adduct from the backside of the serine moiety. The slight

rotation of formoximate around the axis of the phosphor−serine bond P−O4 is also involved in this mode, which implies that the attacking orientation of the oximate would be an important factor to be considered for the reactivation. The atomic distance between P and O1 is 2.634 Å, and the bond length of P−O4 is lengthened to 1.710 Å in the transition state TS1. The Wiberg bond index for P and O1 is evaluated to be 0.09 au, signifying the increasing interaction between these two atoms. The bond index of P−O4 amounts to 0.56 au, and as a comparison, this bond is characterized by the index of 0.65 au in INT1. The attack of the oximate on the phosphorus seems to reduce the strength of the P−O4 bond. The NPA charge for O4 is −0.87 au, only 0.03 au more negative than that in INT1. The charge transfer to this serine oxygen (O4) is insignificant. The free energy of activation between INT1 and TS1 is evaluated to be 6.4 kcal/mol (298 K, 1 atm pressure), which allows the estimation of the reaction rate constant of the nucleophilic attack to be 1.3×10^8 s^{-1}.

From TS1, a penta-coordinated phosphorus intermediate INT2 is located following the intrinsic reaction coordinate (IRC) search. INT2 shows a trigonal bipyramidal (TBP) structure. The methyl and methoxyl groups maintain the similar locations in INT2 as those in INT1 and TS1, which are orientated toward the oximate. This complex is 0.8 kcal/mol less stable than the INT1. A weak bonding between the phosphorus and the oxygen of the oxime (P−O1) is characterized by an atomic distance of 1.951 Å and a bond index of 0.38 au. The P−O4 bond of INT2 is 1.824 Å, 0.17 Å longer than that of INT1. Consistently, the bond index of P−O4 of INT2 (0.46 au) is about 0.2 au smaller than that of INT1. The NPA charges around O1 and O4 are predicted to be −0.65 and −0.88 au, respectively, suggesting that the redistribution of the charges varies more for O1 than for O4.

A very low energy barrier (only 0.1 kcal/mol) needs to be overcome for INT2 to reach the transition state TS2. TS2 also shows a TBP-like structure. Its vibrational mode of the single imaginary frequency ($57i$ cm^{-1}) corresponds to the rotation of the methoxyl group of the sarin moiety from the orientation of the oxime to the orientation of the serine moiety. The bond length of the phosphor−oxime bond P−O1 in TS2 reduces to 1.907 Å as the methoxyl group rotates. Meanwhile, the phosphor−serine bond of P−O4 elongates to 1.863 Å, about 0.2 Å longer than that of INT1. Both of the bond indexes are evaluated to have the same value (0.42 au). The TBP structure intermediate INT3 lies 1.0 kcal/mol below TS2. The atomic distance of the P−O1 bond for INT3 is 1.864 Å (more than 2 Å shorter than that of INT1). The corresponding bond index is strengthened to 0.45 au. The phosphor−serine bond length of P−O4 is calculated to be 1.910 Å, characterized by a smaller bond index (0.39 au) than that in INT1 (0.65 au). Similar to our previous study for the phosphonylation reaction of sarin and AChE,[6] both INT2 and INT3 are stable pentacoordinated phosphorus complexes that are characterized by a unique TBP structure.

The activation energy barrier for the P−O4 bond rupture of INT3 is predicted to be 2.9 kcal/mol (1.9 kcal/mol after the zero point correction). The corresponding transition state (TS3) characterizes the leaving of the serine moiety. The single imaginary frequency of TS3 is $84i$ cm^{-1}, with the vibrational mode characterizing the P−O4 bond cleavage. The atomic distance of P and O4 increases to 2.523 Å, and its bond index is reduced to 0.10 au. The increase of P−O1 bonding is remarkable in this transition state. The phosphor−oxime bond of P−O1 is predicted to be 1.747 Å with a bond index of 0.55 au. The free energy of activation is 1.6 kcal/mol (298 K, 1 atm pressure), and its reaction rate constant is estimated to be 4.1×10^{11} s^{-1}.

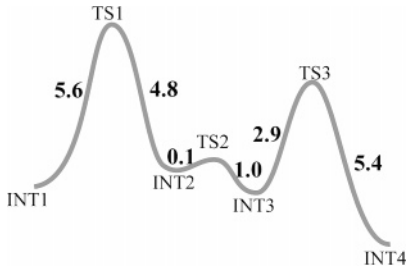

Figure 3. Potential energy surface of reactivation of sarin-inhibited AChE by formoximate anion. (Energy barriers in kcal/mol.)

Through the IRC calculations, the mixture of the products (phosphonylated oxime and serine) of INT4 is located, which is 2.6 kcal/mol more stable than INT1. The bond length of the phosphor−oxime bond P−O1 is shortened to 1.687 Å (about 2 Å shorter than that of INT1), while its bond index is increased significantly to 0.62 au. The atomic distance between the phosphorus and the oxygen O4 of serine amounts to 3.811 Å. Meanwhile, one bifurcated hydrogen bond is noticed for the O4 of serine with two hydrogens from the methyl and the methoxyl groups of sarin moiety, respectively (with atomic distances of 1.946 and 2.027 Å), which is helpful to stabilize the product mixture.

It should be noted that as compared to the energy of the pre-reacting intermediate INT1 (Table 1), the relative energy of the transition state of the nucleophilic attacking step (TS1, 5.6 kcal/mol) is slightly higher than that of the elimination step (TS3, 2.8 kcal/mol).To verify this, the structures of the local minima and the corresponding transition states were re-optimized at the MP2/6-311G(d,p) level of theory. The geometrical parameters obtained at the MP2 level of theory were found to be similar to those predicted at the DFT level (depicted in Figure 2). Compared with the prediction of the density functional theory, the relative energy calculated for the transition state of the nucleophilic attacking process is slightly lower at the MP2 level (4.8 kcal/mol vs 5.6 kcal/mol). On the other hand, the relative energy for the elimination step evaluated by the MP2 approach is close to that of the DFT prediction (2.2 kcal/mol vs 2.8 kcal/mol). Therefore, both density functional theory and the Møller−Plesset perturbation theory concluded that the energy needed for activating the whole reaction is around 6 kcal/mol.

The results discussed previously enable us to establish the potential energy surface along the pathway of the reactivation reaction of sarin-inhibited AChE by the formoximate anion. The entire reaction can occur without difficulty due to the low energy barriers. The potential energy surface is shown in Figure 3. The mechanism of the reactivation includes three connected steps: the anionic formoximate binding to the sarin−serine adduct by bonding with the phosphorus atom, the methoxyl group redirection from the orientation of the oxime moiety to the serine moiety, and the regeneration of serine by cleavage of the phosphor−serine (P−O4) bond. Since the second step of the rotation of the methoxyl group is nearly barrierless, the whole reactivation reaction can be considered a mainly two-step process, of which the elimination step to regenerate serine is competitive with the nucleophilic attacking process of oxime on the sarin−serine adduct.

To evaluate the influences of the solvent effects on the studied reaction, based upon the gas-phase optimization structures, the polarizable continuum model (PCM) for the aqueous solution was applied at the B3LYP/6-311G(d,p) theoretical level. The

results (Table 1) show that the energy barrier for the first step (nucleophilic attack) is lowered to 4.1 kcal/mol, while the activation energy for the departure of serine is raised to 5.9 kcal/mol, implying that ~3 kcal/mol more energy will be needed to accomplish the elimination step for the recovery of the serine moiety in water than is necessary in the gas phase.

Conclusion

The potential energy surface along the pathway of the reactivation reaction of sarin-inhibited AChE by formoximate anion has been explored by applying the DFT approach at the B3LYP/6-311G(d,p) level and the Møller−Plesset perturbation theory at the MP2/6-311G(d,p) level. The mechanism is proposed to undergo a mainly two-step process, in which the formoximate binds to the sarin-AChE adduct to form a relatively stable phosphorus complex and the regeneration of the serine occurs subsequently. The two steps are competitive in the entire pathway. The reaction can occur fast and effortlessly due to the relatively low energy barriers. The polarizable continuum model (PCM) has been applied to evaluate the solvate effects on the studied pathway. The results derived from both the gas-phase model and the aqueous solvation model suggest that the studied oximate anion could be a promising antidote reagent for the sarin-inhibited AChE.

Acknowledgment. This work was supported by a CMCM grant (2T34GM007672-25A1) and by the Army High Performance Computing Research Center under the auspices of the Department of the Army, Army Research Laboratory cooperative agreement DAAD19-01-2-0014, the content of which does not necessarily reflect the position or the policy of the government, and no official endorsement should be inferred. We are also thankful to the Mississippi Center for Supercomputing Research for use of the computational facility.

References and Notes

(1) Rosenberry, T. L. In *Advances in Enzymology*; Meister, A., Ed.; Wiley and Sons: New York, 1975; Vol. 43, pp 103−218.

(2) Quinn, D. M. *Chem. Rev.* **1987**, *87*, 955−975.

(3) Sussman, J. L.; Harel, M.; Frolow, F.; Oefner, C.; Goldman, A.; Toker, L.; Silman, I. *Science* **1991**, *253*, 872.

(4) Taylor, P.; Lappi, S. *Biochemistry* **1975**, *14*, 1989−1997.

(5) Harel, M.; Schalk, I.; Ehret-Sabatier, L.; Bouet, F.; Goeldner, M.; Hirth, C.; Axelsen, P. H.; Silman, I.; Sussman, J. L. *Proc. Natl. Acad. Sci. U.S.A.* **1993**, *90*, 9031−9035.

(6) Wang, J.; Gu, J.; Leszczynski, J. *J. Phys. Chem. B* **2006**, *110*, 7567−7573.

(7) Wang, J.; Roszak, S.; Gu, J.; Leszczynski, J. *J. Phys. Chem. B* **2005**, *109*, 1006−1014.

(8) Morales-Rojas, H.; Moss, R. A. *Chem. Rev.* **2002**, *102*, 2497−2521.

(9) Buncel, E.; Cannes, C.; Chatrousse, A.-P.; Terrier, F. *J. Am. Chem. Soc*. **2002**, *124*, 8766−8767 and references therein.

(10) Patočka, J.; Cabal, J.; Kuča, K.; Jun, D. *J. Appl. Biomed.* **2005**, *3*, 91−99.

(11) Kovach, I. M.; Bennet, A. J.; Bibbs, J. A.; Zhao, Q. *J. Am. Chem. Soc.* **1993**, *115*, 5138−5144.

(12) Luo, C.; Saxena, A.; Smith, M.; Garcia, G.; Radiæ, Z.; Taylaor, P.; Doctor, B. P. *Biochemistry* **1999**, *38*, 9937−9947.

(13) Wong, L.; Radiæ, Z.; Brüggemann, R. J. M.; Hosea, N.; Berman, H. A.; Taylor, P. *Biochemistry* **2000**, *39*, 5750−5757.

(14) Kuča, K.; Bartošová, L.; Jun, D.; Patočka, J.; Cabal, J.; Kassa, J.; Kunešová, G. *Biomed. Papers* **2005**, *149*, 75−82.

(15) Becke, A. D. *J. Chem. Phys.* **1993**, *98*, 5648−5652.

(16) Lee, C.; Yang, W.; Parr, R. G. *Phys. Rev. B* **1988**, *37*, 785−789.

(17) Miehlich, B.; Savin, A.; Stoll, H.; Preuss, H. *Chem. Phys. Lett.* **1989**, *157*, 200−206.

(18) Hehre, W. J.; Radom, L.; Schleyer, P. R.; Pople, J. A. *Ab Initio Molecular Orbital Theory*; Wiley and Sons: New York, 1986.

(19) Binkley, J. S.; Pople, J. A. *Int. Quantum Chem.* **1975**, *9*, 229−236.

(20) Reed, A. E.; Weinstock, R. B.; Weinhold, F. *J. Chem. Phys.* **1985**, *83*, 735.

(21) Reed, A. E.; Weinhold, F. *J. Chem. Phys.* **1985**, *83*, 1736.

(22) Reed, A. E.; Curtiss, L. A.; Weinhold, F. *Chem. Rev.* **1988**, *88*, 899.

(23) Reed, A. E.; Schleyer, P. R. *J. Am. Chem. Soc*. **1990**, *112*, 1434.

(24) Frisch, M. J.; Trucks, G. W.; Schlegel, H. B.; Scuseria, G. E.; Robb, M. A.; Cheeseman, J. R.; Montgomery, J. A., Jr.; Vreven, T.; Kudin, K. N.; Burant, J. C.; Millam, J. M.; Iyengar, S. S.; Tomasi, J. Barone, V.; Mennucci, B.; Cossi, M.; Scalmani, G.; Rega, N.; Petersson, G. A.; Nakatsuji, H.; Hada, M.; Ehara, M.; Toyota, K.; Fukuda, R.; Hasegawa, J.; Ishida, M.; Nakajima, T.; Honda, Y.; Kitao, O.; Nakai, H.; Klene, M.; Li, X.; Knox, J. E.; Hratchian, H. P.; Cross, J. B.; Adamo, C.; Jaramillo, J.; Gomperts, R.; Stratmann, R. E.; Yazyev, O.; Austin, A. J.; Cammi, R.; Pomelli, C.; Ochterski, J. W.; Ayala, P. Y.; Morokuma, K.; Voth, G. A.; Salvador, P.; Dannenberg, J. J.; Zakrzewski, V. G.; Dapprich, S.; Daniels, A. D.; Strain, M. C.; Farkas, O.; Malick, D. K.; Rabuck, A. D.; Raghavachari, K.; Foresman, J. B.; Ortiz, J. V.; Cui, Q.; Baboul, A. G.; Clifford, S.; Cioslowski, J.; Stefanov, B. B.; Liu, G.; Liashenko, A.; Piskorz, P.; Komaromi, I.; Martin, R. L.; Fox, D. J.; Keith, T.; Al-Laham, M. A.; Peng, C. Y.; Nanayakkara, A.; Challacombe, M.; Gill, P. M. W.; Johnson, B.; Chen, W.; Wong, M. W.; Gonzalez, C.; Pople, J. A. *Gaussian 03*, revision C.02; Gaussian, Inc.: Pittsburgh, PA, 2003.

(25) Cossi, M.; Barone, V.; Cammi, R.; Tomasi, J. *Chem. Phys. Lett.* **1996**, *255*, 327−335.

(26) Bruice, T. C. *Chem. Rev.* **2006**, *106*, 3119−3139.